

Structural basis for the killing of human beta cells by CD8⁺ T cells in type 1 diabetes

Anna M Bulek^{1,9}, David K Cole^{1,9}, Ania Skowera^{2,3,9}, Garry Dolton¹, Stephanie Gras⁴, Florian Madura¹, Anna Fuller¹, John J Miles^{1,5}, Emma Gostick¹, David A Price¹, Jan W Drijfhout⁶, Robin R Knight², Guo C Huang⁷, Nikolai Lissin⁸, Peter E Molloy⁸, Linda Wooldridge¹, Bent K Jakobsen⁸, Jamie Rossjohn^{1,4}, Mark Peakman^{2,3,9}, Pierre J Rizkallah^{1,9} & Andrew K Sewell^{1,9}

The structural characteristics of the engagement of major histocompatibility complex (MHC) class II-restricted self antigens by autoreactive T cell antigen receptors (TCRs) is established, but how autoimmune TCRs interact with complexes of self peptide and MHC class I has been unclear. Here we examined how CD8⁺ T cells kill human islet beta cells in type 1 diabetes via recognition of a human leukocyte antigen HLA-A*0201-restricted glucose-sensitive preproinsulin peptide by the autoreactive TCR 1E6. Rigid 'lock-and-key' binding underpinned the 1E6-HLA-A*0201-peptide interaction, whereby 1E6 docked similarly to most MHC class I-restricted TCRs. However, this interaction was extraordinarily weak because of limited contacts with MHC class I. TCR binding was highly peptide centric, dominated by two residues of the complementarity-determining region 3 (CDR3) loops that acted as an 'aromatic-cap' over the complex of peptide and MHC class I (pMHCI). Thus, highly focused peptide-centric interactions associated with suboptimal TCR-pMHCI binding affinities might lead to thymic escape and potential CD8⁺ T cell-mediated autoreactivity.

The locus on human chromosome 6 that encodes the major histocompatibility complex (MHC) is the most important genetic locus for human autoimmune diseases, which indicates that the recognition of self antigens by T cells initiates and drives pathology^{1,2}. Most, but evidently not all, self-reactive T cells are eliminated in the thymus by negative selection³. Hence, there is a pressing need to better understand the molecular interactions through which disease-relevant T cell antigen receptors (TCRs) bind to ligands consisting of complexes of self-derived peptide and MHC (self-pMHC) and escape thymic negative selection to populate the periphery. Structural studies of many non-autoimmune complexes of TCR and peptide-MHC (TCR-pMHC) have demonstrated that this can be a variable and versatile interaction⁴⁻¹⁴ in which a prototypic diagonal TCR-pMHC docking mode is used with the α - and β -chain variable-region domains of the TCR positioned over the $\alpha 2$ and $\alpha 1$ helices of the MHC molecule, respectively^{4,15}. In contrast, at present the structural database for human autoantigen-reactive TCRs in complex with their self ligands is very limited. Three complexes show atypical binding properties relative to that of pathogen-specific TCR-pMHC complexes^{13,16,17}, such as a predominant focus on the amino-terminal region of the peptide or excessive tilting^{13,16}, which has led to the proposal that autoreactive TCRs have an abnormal docking mode. However, only four structures

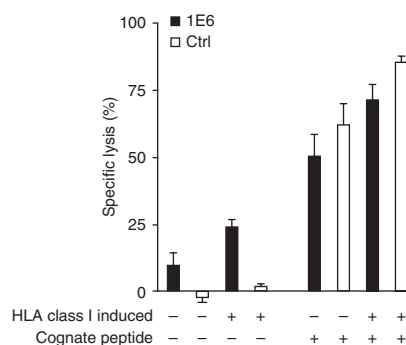
in total have been described so far, and all are restricted to MHC class II and specific for myelin basic protein (MBP)^{13,14,16,17}, an auto-antigen targeted in multiple sclerosis. At present, no structural or molecular data exist for other human autoimmune diseases. More notably, there has been no exploration of the molecular interaction between an autoreactive TCR and a complex of self peptide and MHC class I (self-pMHCI) displayed on the surface of a target cell that is destroyed as the central component of autoimmune disease pathology.

To address that knowledge gap, we turned to type 1 diabetes, an organ-specific autoimmune disease focused on the islets of Langerhans, in which beta cells are destroyed, which leads to lifelong insulin dependence. Genome-wide association studies have demonstrated a key role for genes encoding MHC class I in determining disease susceptibility (those encoding the human leukocyte antigens HLA-A*02, HLA-B*18, HLA-A*24 and HLA-B*39)¹ with a relative risk similar to or greater than that of more classically associated genes such as *INS* (which encodes preproinsulin (PPI)) and *PTPN22* (which encodes the lymphoid tyrosine phosphatase PTPN22 (Lyp)). As the main role of MHC class I is to present peptide antigens to CD8⁺ cytotoxic T lymphocytes, there are sound reasons for proposing that CD8⁺ T cells specific for beta cell-derived peptides, presented by MHC class I molecules, have a pivotal role in beta-cell destruction. Indeed, CD8⁺

¹Institute of Infection and Immunity, Cardiff University School of Medicine, Heath Park, Cardiff, UK. ²Department of Immunobiology, King's College London, London, UK. ³National Institute for Health Research, Biomedical Research Centre at Guy's & St. Thomas' National Health Service Foundation Trust and King's College London, London, UK. ⁴The Protein Crystallography Unit, Department of Biochemistry and Molecular Biology, School of Biomedical Sciences, Monash University, Clayton, Australia. ⁵Cellular Immunology Laboratory, Queensland Institute of Medical Research, Brisbane, Australia. ⁶Department of Immunohematology and Blood Transfusion, Leiden University Medical Centre, Leiden, The Netherlands. ⁷Diabetes and Nutritional Science, King's College London, London, UK. ⁸Immunocore, Abingdon, UK. ⁹These authors contributed equally to this work. Correspondence should be addressed to A.K.S. (sewellak@cardiff.ac.uk).

Received 2 September 2011; accepted 6 December 2011; published online 15 January 2012; doi:10.1038/ni.2206

Figure 1 The CD8⁺ T cell clone 1E6 kills unmanipulated human islets from various donors without any requirement for cytokine treatment or the addition of exogenous cognate self peptide. Specific lysis of human islet cells from HLA-A*0201⁺ organ donors, cultured with 1E6 T cells (restricted to HLA-A*0201 specific for PPI amino acids 15–24) or a CD8⁺ T cell clone specific for a peptide consisting of amino acids 495–503 of cytomegalovirus polypeptide pp65 (control (Ctrl)), and parallel control experiments in the presence of exogenous cognate peptide (bottom row). Data are from three studies with three different donors (mean and s.e.m. of triplicates).



T cells dominate the characteristic islet mononuclear-cell infiltrate observed after death in patients studied close to diagnosis¹⁸ and are required to mediate efficient adoptive transfer of disease in animal models¹⁹. A CD8⁺ T cell clone (1E6) specific for the major beta-cell autoantigen PPI has been generated from a blood sample obtained from a patient studied 3 months after the onset of type 1 diabetes, diagnosed according to criteria of the American Diabetes Association and including acute onset of symptoms, glycosuria, random plasma glucose concentration measurement of >11.1 mmol/l and positivity for autoantibodies to the glutamic acid decarboxylase GAD65 (ref. 20). The 1E6 clone mediates beta cell-specific killing via recognition of a highly distinctive signal peptide epitope (amino acids 15–24 of PPI) presented by HLA-A*0201 that shows glucose-dependent presentation on the surface of human beta cells²⁰. The contact between the TCR of this clone and self-pMHC1 on the beta-cell surface is thus representative of a critical, disease-determining molecular interaction in a common human autoimmune disease. Here we present the structures of the TCR expressed by the beta cell-specific cytotoxic CD8⁺ T cell clone 1E6, its cognate antigen HLA-A*0201-ALWGPDPAAA (A2-ALW), and the 1E6-A2-ALW complex. This structure of an autoreactive TCR-self-pMHC1 complex furthers the understanding of how autoreactive T cells may escape into the periphery by demonstrating a previously unknown mechanism for the recognition of an MHC class I-restricted self antigen by an autoreactive TCR.

RESULTS

T cell clone 1E6 kills human islet cells with high sensitivity

To confirm the role of 1E6 T cells in type 1 diabetes, we extended published studies of 1E6-mediated killing²⁰ through the use of human islet cells purified from three additional HLA-A*0201⁺ organ donors. Robust killing has been reported for islet cells pretreated with cytokines as a means to increase HLA-A*0201 surface expression²⁰, which recapitulates the well-described islet hyperexpression of MHC class I seen in human type 1 diabetes²¹. However, here we found that

untreated islet cells with resting amounts of MHC class I expression and without the addition of exogenous PPI peptide (amino acids 15–24) were also highly sensitive to killing by 1E6 T cells (**Fig. 1**). We observed killing by 1E6 cells in the absence of cytokine treatment; this was enhanced in islets pretreated with cytokines to induce expression of HLA class I (**Supplementary Fig. 1**). These data demonstrated that 1E6 T cells were able to engage with naturally occurring amounts of self-pMHC1 ligand (**Supplementary Fig. 1**) and were able to mediate disease-related effector functions as a consequence. Moreover, the circulation of most patients with type 1 diabetes showed enrichment for CD8⁺ T cells with specificity for this key beta-cell target, as demonstrated by enzyme-linked immunospot analysis of interferon- γ ²⁰ and staining of peripheral blood lymphocytes with a multimer of HLA-A*0201 (A2-ALW) loaded with amino acids 15–24 of PPI²², and these CD8⁺ T cells had a 'preferential' effector memory phenotype (data not shown). Thus, beta cell-reactive CD8⁺ T cells specific for A2-ALW probably mediate important effector functions in patients with type 1 diabetes²⁰.

A central Gly-Pro-Asp motif governs recognition by 1E6

Next we probed the specificity of 1E6 T cells with a comprehensive peptide-mutagenesis scan. We used the index ALWGPDPAAA sequence as a template and systematically substituted each residue along the backbone with all other 19 amino acids. We assessed the production of tumor necrosis factor as the activation 'readout'. By this approach, we found that the 1E6 TCR was tolerant to changes in peptide residues Ala1, Leu2, Ala8, Ala9 and Ala10; in some cases, substitution at these residues generated larger responses than that generated by the index peptide (for example, substitution of Ala1 with Arg1, and Leu2 with Gln2; **Fig. 2**). Modifications of anchor residues can directly alter TCR binding affinity and T cell sensitivity²³; thus,

| Index | A | L | W | G | P | D | P | A | A | A |
|-------|------------|------------|------------|------------|------------|------------|------------|------------|------------|-------------|
| | Position 1 | Position 2 | Position 3 | Position 4 | Position 5 | Position 6 | Position 7 | Position 8 | Position 9 | Position 10 |
| A | 100 | 133 | 48 | 51 | 17 | 35 | 24 | 100 | 100 | 100 |
| F | 37 | 9 | 16 | 19 | 19 | 0 | 10 | 0 | 65 | 1 |
| I | 126 | 80 | 22 | 39 | 15 | 0 | 24 | 79 | 45 | 74 |
| L | 29 | 100 | 14 | 30 | 7 | 0 | 18 | 135 | 18 | 224 |
| M | 44 | 207 | 10 | 34 | 24 | 16 | 0 | 132 | 99 | 32 |
| P | 41 | 0 | 45 | 34 | 100 | 14 | 100 | 81 | 83 | 0 |
| V | 265 | 29 | 10 | 12 | 21 | 24 | 0 | 1 | 20 | 48 |
| W | 41 | 0 | 100 | 23 | 0 | 12 | 0 | 113 | 0 | 0 |
| Y | 161 | 21 | 50 | 20 | 0 | 9 | 0 | 128 | 28 | 0 |
| C | 44 | 0 | 28 | 27 | 20 | 0 | 19 | 79 | 60 | 45 |
| G | 261 | 15 | 26 | 100 | 16 | 0 | 11 | 77 | 12 | 0 |
| N | 158 | 0 | 30 | 16 | 21 | 11 | 0 | 313 | 24 | 0 |
| Q | 69 | 282 | 50 | 29 | 0 | 16 | 0 | 19 | 64 | 4 |
| S | 87 | 35 | 27 | 20 | 0 | 28 | 0 | 28 | 38 | 0 |
| T | 84 | 116 | 8 | 21 | 0 | 19 | 0 | 8 | 63 | 24 |
| D | 0 | 0 | 36 | 18 | 16 | 100 | 13 | 7 | 0 | 0 |
| E | 0 | 0 | 23 | 22 | 9 | 0 | 15 | 0 | 0 | 0 |
| H | 85 | 0 | 39 | 49 | 24 | 0 | 20 | 78 | 0 | 14 |
| K | 287 | 0 | 21 | 28 | 16 | 0 | 19 | 245 | 57 | 0 |
| R | 320 | 0 | 41 | 20 | 0 | 21 | 0 | 129 | 29 | 0 |

Figure 2 Mutational scan of the 1E6 CD8⁺ T cell clone. Peptide-mutagenesis scan assessing the induction of the secretion of tumor necrosis factor from 1E6 CD8⁺ T cells induced by peptides with single substitutions (presented in one-letter code) of each of the 10 positions in the self peptide ALWGPDPAAA (index peptide) with each of the 19 other proteogenic amino acids, normalized to the response induced by the index peptide (yellow), set as 100: pink, substitutions that resulted in a response of below 25 compared with index sequence; orange, nonpolar hydrophobic substitutions; green, polar hydrophobic substitutions; blue, polar uncharged substitutions; red, acidic substitutions; white, basic substitutions. Data are from three experiments (average).

Table 1 Binding affinity of 1E6-ALW complex

| Temperature (°C) | K_d (μM) | ΔG_0 (kcal/mol) |
|------------------|-------------------------|-------------------------|
| 5 | 274.5 ± 14 | -4.5 |
| 25 | 278 ± 7.6 | -4.8 |
| 37 | 335 ± 44 | -4.9 |

K_d , dissociation constant; ΔG_0 , Gibbs free energy at time 0. Data are representative of four experiments (mean \pm s.e.m.).

the enhanced responses observed could have reflected, at least in part, indirect modifications to the conformation of the peptide that aid TCR binding. In contrast, modifications to the central Gly-Pro-Asp motif were not well tolerated. Modifications to this region of the peptide resulted in activation that was at least half as great in all instances, whereas changes to other regions of the peptide were much less critical and in some cases resulted in more activation than that obtained with the wild-type sequence. This was consistent with published structural data showing that TCRs generally focus on the central residues of the peptide, which typically bulge out of the MHC groove^{4,15}. Overall, the functional mutagenesis scan demonstrated the critical importance of the central Gly-Pro-Asp motif in peptide recognition by the 1E6 CD8⁺ T cell clone.

The 1E6 TCR binds very weakly to A2-ALW

We next determined the affinity of the 1E6-A2-ALW interaction by analysis of surface plasmon resonance (SPR). Typically the affinity of a pathogen-specific TCR-pMHCI interaction is in the region of 1–10 μM (ref. 24). In contrast, the binding affinity of the 1E6-A2-ALW interaction was very low (a dissociation constant of $\sim 278 \mu\text{M} \pm 7.6 \mu\text{M}$ at 25 °C), with kinetics that were too rapid to measure (Table 1 and Supplementary Fig. 2). To confirm that this weak interaction was not temperature dependent, we also measured the binding affinity at 5 °C (dissociation constant, $\sim 274.5 \mu\text{M}$) and 37 °C (dissociation constant, $\sim 335 \mu\text{M}$); the latter reflected physiological conditions (Table 1). Thus, similar to some other interactions of TCRs with self peptide-MHC class II^{17,24}, the affinity of this MHC class I-restricted autoreactive TCR was very low and within the overall spectrum of TCR-pMHCI interactions for which biophysical data are available. Indeed, to our knowledge, this is the lowest TCR-pMHCI affinity recorded for any natural human agonist ligand.

The 1E6 TCR binds pMHC in a canonical orientation

To investigate the structural basis of a CD8⁺ T cell response to an HLA-A*0201-restricted, PPI-derived epitope, we solved the structure of the 1E6 TCR in complex with A2-ALW in two different crystal forms at a resolution of 2.6 Å and 2.7 Å (Supplementary Table 1). The ternary complexes were almost completely identical in the two different crystal forms and thus we restricted our analysis to the complex solved at a higher resolution. The electron density at the interface was unambiguous, which permitted structural analysis (Supplementary Fig. 3). Furthermore, we solved the structures of the binary A2-ALW complex and the 1E6 TCR not in complex to resolutions of 1.7 Å and 2.6 Å, respectively (Supplementary Table 1), which enabled assessment of the degree of conformational change that took place after complex formation. Indeed, whereas plasticity of either the TCR and/or the peptide is a hallmark of the TCR-pMHC interaction^{8,12,25,26}, neither the 1E6 TCR nor the A2-ALW complex moved appreciably during ligation. This indicated that the 1E6 autoreactive TCR engaged the self-pMHCI in a rigid 'lock-and-key' manner (Supplementary Figs. 4 and 5).

Contrary to reports that some autoimmune TCRs bind to self-pMHC complexes with atypical docking modes^{13,16,17}, the 1E6 TCR bound in a conventional, centrally located orientation, with the TCR α -chain positioned over the $\alpha 2$ helix of MHC class I and the TCR β -chain positioned over the $\alpha 1$ helix of MHC class I (Fig. 3a). Indeed, the docking angle of 58.4° for the TCR (calculated as reported before⁴) for the 1E6-A2-ALW complex was within the range observed for other human TCR-pMHC complexes (32°–80°), with the 1E6 TCR located over the solvent-exposed Gly-Pro-Asp bulge of the ALW peptide (Fig. 3a,b). The surface-complementarity index across the interface was 0.61, which was also in the normal range for TCR-pMHCI complexes (0.60–0.72)¹¹. Further, the total buried surface area of the 1E6-A2-ALW complex was 1,640 Å², at the lower end of the range observed for human TCR-pMHCI complexes (1,470–2,450 Å²). Thus, the 1E6-A2-ALW complex had overall characteristics typical of most previously determined TCR-pMHCI structures.

Recognition by the 1E6 TCR involves limited MHC contacts

Although in most TCR-pMHC structures solved so far the number of TCR contacts with peptide is less than the number of contacts with the restricting MHC molecule⁴, the 1E6-A2-ALW interaction was unusually peptide centric (discussed below) with a footprint with more limited MHC contact than that of other antipathogen TCR-pMHCI structures. For example, the crystal structure of the AS01 TCR in complex with the HLA-A*0201-restricted, Epstein Barr virus-derived antigen A2-GLC (the GLCTLVAML (GLC) peptide from the Epstein Barr virus protein BMLF1)¹¹ demonstrated far broader TCR interactions with both the MHC surface and the peptide (Fig. 3c,d). Comparison of the surface contacts of the 1E6 and AS01 TCRs

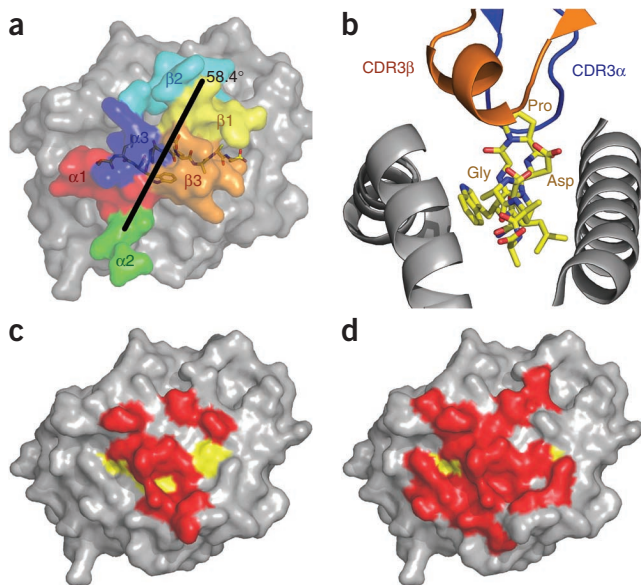


Figure 3 Binding interface of 1E6-A2-ALW. (a) Positions of the 1E6 TCR CDR loops (red, CDR1 α ; green, CDR2 α ; blue, CDR3 α ; yellow, CDR1 β ; cyan, CDR2 β ; orange, CDR3 β) in the structure of the complex of the 1E6 TCR and ALW (yellow sticks) bound to HLA-A*0201 (gray surface). Black diagonal line indicates the crossing angle of the TCR (58.4°). (b) View down the center of the MHC binding groove (ALW; yellow sticks) showing the perpendicular binding conformation of the TCR CDR3 α loop (blue) and CDR3 β loop (orange). (c) Surface representation of the binding footprint of the 1E6 TCR over A2-ALW (A2, gray surface; ALW, yellow surface); red indicates A2-ALW residues contacted by the 1E6 TCR. (d) Surface representation of the binding footprint of the AS01 TCR over A2-GLC¹¹ (A2, gray surface; GLC, yellow surface); red indicates A2-GLC residues contacted by the AS01 TCR, calculated with a cutoff of 3.2 Å for hydrogen bonds and a cutoff of 4 Å for van der Waals contacts.



Table 2 Contacts between the 1E6 TCR and A2-ALW

| CDR loop | Gene | TCR residue | Peptide residue | MHC residue | van der Waals contacts | Hydrogen bonds |
|---------------|--------------------|----------------------|-------------------|----------------------|------------------------|----------------|
| CDR3 α | <i>TRAV12-3</i> | Arg92 | Pro5 | | 1 | |
| | <i>TRAJ12</i> | Asp94 | | Lys66 | 2 | |
| | <i>TRAJ12</i> | Asp94 ⁰⁸² | | Lys66 ^{NC} | | 1 salt bridge |
| | <i>TRAJ12</i> | Asp94 | Gly4 | | 4 | |
| | <i>TRAJ12</i> | Asp94 | Pro5 | | 6 | |
| | <i>TRAJ12</i> | Asp94 ⁰ | Pro5 ^N | | | 1 |
| | <i>TRAJ12</i> | Ser95 | | Arg65 | 1 | |
| | <i>TRAJ12</i> | Ser95 ⁰⁶ | | Arg65 ^{NH2} | 1 | 1 |
| | <i>TRAJ12</i> | Ser95 | | Lys66 | 1 | |
| | <i>TRAJ12</i> | Ser95 | Pro5 | | 2 | |
| | <i>TRAJ12</i> | Ser96 | | Arg65 | 3 | |
| | <i>TRAJ12</i> | Ser96 | Pro5 | | 4 | |
| | <i>TRAJ12</i> | Tyr97 | Pro5 | | 10 | |
| | <i>TRAJ12</i> | Tyr97 | Asp6 | | 5 | |
| CDR1 β | <i>TRBV12-4</i> | Tyr31 | | | 2 | |
| | <i>TRBV12-4</i> | Tyr31 ^{0H} | Asp6 ⁰ | | | 1 |
| CDR2 β | <i>TRBV12-4</i> | Asn50 | | Gln72 | 1 | |
| | <i>TRBV12-4</i> | Asn51 | | Val76 | 1 | |
| | <i>TRBV12-4</i> | Val53 | | Gln72 | 3 | |
| | <i>TRBV12-4</i> | Ile55 | | Arg65 | 2 | |
| | <i>TRBV12-4</i> | Asp56 | | Arg65 | 2 | |
| CDR3 β | <i>TRBD2-2 + N</i> | Trp97 | | Ala150 | 2 | |
| | <i>TRBD2-2 + N</i> | Trp97 | | Val152 | 2 | |
| | <i>TRBJ2-4</i> | Ala101 | | Gln155 | 1 | |
| | <i>TRBJ2-4</i> | Lys102 | | His151 | 3 | |
| | <i>TRBD2-2 + N</i> | Trp97 | Asp6 | | 4 | |
| | <i>TRBD2-2 + N</i> | Trp97 ^{Ne1} | Asp6 ⁰ | | | 1 |
| | <i>TRBD2-2 + N</i> | Trp97 | Pro7 | | 6 | |
| | <i>TRBD2-2 + N</i> | Trp97 ^{Ne1} | Pro7 ⁰ | | | 1 |
| | <i>TRBD2-2 + N</i> | Trp97 | Ala8 | | 9 | |
| | <i>TRBD2-2 + N</i> | Trp97 ^{Ne1} | Ala8 ^N | | | 1 |

A cutoff of 3.4Å was used for hydrogen bonds and salt bridges, and a cutoff of 4Å was used for van der Waals contacts. Superscripted designations indicate the element involved in hydrogen bonding or salt bridges; '+ N' indicates insertion of nongermline nontemplated nucleotide(s) during V(D)J rearrangement.

demonstrated that the 1E6 TCR implemented a more focused minimal contact zone when binding to A2-ALW. On average, human TCRs make about 4 hydrogen bonds and ~66 van der Waals contacts with the MHC surface⁴. A TCR bound to a superbulged 13-residue peptide made the fewest contacts with MHC seen so far⁴, with only 2 hydrogen bonds, 1 salt bridge and 36 van der Waals contacts with the MHC (calculated independently with a cutoff of 4Å or less for van der Waals contacts and a cutoff of 3.4Å or less for hydrogen bonds and salt bridges)²⁷. In comparison, the 1E6 TCR formed only 1 hydrogen bond, 1 salt bridge and 24 van der Waals contacts with the MHC (Table 2). At the interface, only the complementarity-determining region 3 α -loop (CDR3 α) of the TCR interacted with the MHC surface, whereas both the CDR2 β and CDR3 β loops made MHC contacts (Fig. 4a). The CDR3 α loop used its residue Asp94 to make one salt bridge and two van der Waals contacts with MHC residue Lys66; Ser95 α to make one hydrogen bond and one van der Waals contact with Arg65 and a solitary van der Waals contact with Lys66; and Ser96 α to make three van der Waals contacts with Arg65 (Table 2 and Fig. 4b,c). Trp97 β of the CDR3 β loop made a network of two van der Waals contacts each with MHC residues Ala150 and Val152. In addition, there was one van der Waals contact between Ala101 β of CDR3 β and MHC residue Gln155, and three van der Waals contacts between Lys102 β of CDR3 β and MHC residue His151 (Table 2 and Fig. 4b,c). The TCR CDR2 β loop contacted the MHC through a total of nine van der Waals interactions, comprising one van der Waals contact between Asn50 β of CDR2 β and Gln72 of the MHC; one van der Waals contact between Asn51 β of CDR2 β and Val76 of the MHC; three van der Waals contacts between Val53 β of

CDR2 β and Gln72 of the MHC; two van der Waals contacts between Ile55 β of CDR2 β and Arg65 of the MHC; and two van der Waals contacts between Asp56 β of CDR2 β and Arg65 of the MHC. The prominent role of the CDR3 loops, especially the CDR3 α loop, in contacting the MHC was in contrast to the present view that the germline-encoded CDR1 and CDR2 loops govern interactions with the MHC^{28,29}.

Published TCR-pMHC structural analyses have demonstrated the existence of three conserved MHC contact points (positions 65, 69 and 155; the 'restriction triad')²⁷, although the dependence of these positions in mediating TCR recognition is not absolute⁴. Of the nine MHC residues contacted by the TCR, Arg65 made a sizeable network of interactions with both the TCR α -chain and the TCR β -chain. However, although Arg65 was a chief MHC residue contacted by the 1E6 TCR, only one van der Waals contact (>3.4Å) was formed with the MHC 'gatekeeper' residue Gln155, and no contacts were made with the other restriction triad residue, Arg69. This suggests that for this autoreactive TCR-self-pMHC complex, contacting the conserved 'triad' was not obligatory for productive engagement³⁰.

Focused peptide-centric recognition

In contrast to typical TCR recognition of MHC molecules bound to peptides eight to ten amino acids in length⁴, the 1E6 TCR

formed more peptide-mediated contacts than MHC interactions. Specifically, six of eight (75%) of the hydrogen bonds and salt bridges, and 53 of 77 (69%) of the van der Waals contacts, were between the TCR and the self peptide (Table 2). The TCR α -chain used only its CDR3 α loop to contact the self peptide, forming a total of 2 hydrogen bonds and 32 van der Waals contacts, whereas the TCR β -chain bound the peptide via its CDR1 β and CDR3 β loops, forming a total of 4 hydrogen bonds and 21 van der Waals contacts. The central positioning of the 1E6 TCR over the ALWGPDPAAA peptide enabled contacts with the central five amino acids (Gly-Pro-Asp-Pro-Ala) of the self

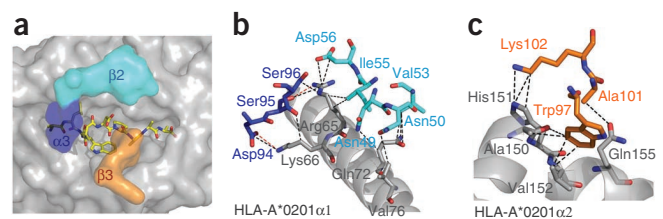


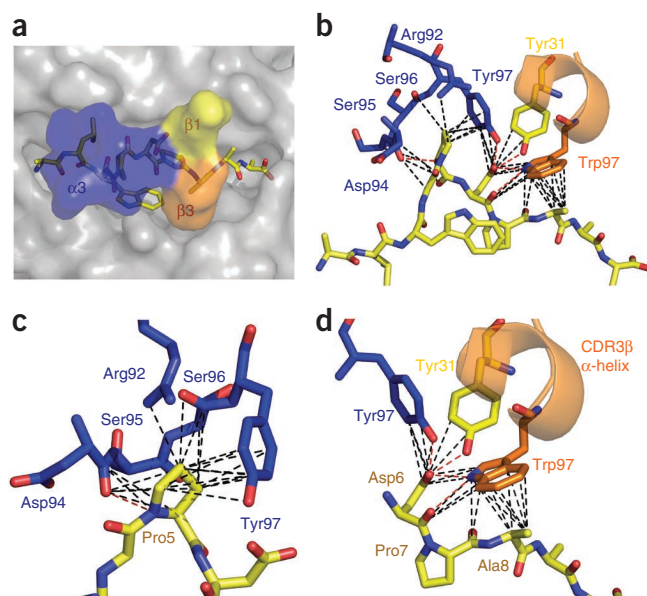
Figure 4 Interactions of the 1E6 TCR with HLA-A*0201. (a) Surface representation of residues of the TCR CDR loops (blue, CDR3 α ; cyan, CDR2 β ; orange, CDR3 β) that contacted the MHC surface. (b) Contacts between the TCR and the MHC α 1 helix domain, showing the van der Waals contacts (black dashed lines) and hydrogen bonds (red dashed lines) made by the TCR CDR3 α , CDR2 β and CDR3 β loops with the MHC α 1 helix central domain, including residue Arg65, which is part of the MHC 'restriction triad'. (c) Contacts (stabilizing interactions) between the TCR β -chain CDR3 β loop and the MHC α 2 helix domain, including a van der Waals contact with the 'gatekeeper' residue Gln155 of MHC.

Figure 5 Interactions of the 1E6 TCR with ALW. (a) Surface representation of the TCR residues (blue, CDR3 α ; yellow, CDR1 β ; orange, CDR3 β) that contact ALW (yellow sticks). (b) Main contacts between the TCR and ALW, showing van der Waals contacts (black dashed lines) and hydrogen bonds (red dashed lines) between the TCR CDR3 α , CDR1 β and CDR3 β loops and ALW. (c) Contacts between ALW Pro5 (yellow sticks) and the TCR CDR3 α loop (blue sticks). (d) Contacts between the TCR CDR1 β and CDR3 β loops and the C terminus of ALW in which Asp6 was the main contact residue, as well as the dominant role of the TCR β -chain residue Trp97 (orange sticks) during binding of the self peptide. Trp97 is the only CDR3 β loop residue in contact with the peptide, making many van der Waals contacts and hydrogen bonds with Asp6, Pro7 and Ala8 of ALW.

peptide (Fig. 5a,b). The TCR CDR3 α and CDR3 β loops formed a tight binding pocket around the Gly-Pro-Asp motif and accounted for most of the contacts of the self peptide, whereas the CDR1 β loop served a lesser role during binding of the self peptide (Fig. 5b). Whereas the 1E6 TCR was positioned in a canonical diagonal way over A2-ALW (Fig. 3a), the CDR3 loops of the 1E6 TCR were twisted into a perpendicular orientation over the self peptide, which enabled the formation of more TCR contacts with Pro5 (Fig. 3b). Although the 1E6 TCR interacted with 50% of the residues in the self peptide, most of the interactions were focused in a contact zone that included just two residues: Pro5 and Asp6. Indeed, Pro5 and Asp6 accounted for four of six of the hydrogen bonds and 34 of 53 of the van der Waals contacts between the TCR and the self peptide (Table 2 and Fig. 5c,d). The prominent exposed central position of Pro5 resulted in many contacts between the TCR and the ALW peptide. Pro5 formed one hydrogen bond with TCR residue Asp94 α and a notable network of 23 van der Waals interactions with Arg92 α , Asp94 α , Ser95 α and Tyr97 α in the TCR CDR3 α loop (Fig. 5c). Asp6 formed one hydrogen bond and five van der Waals contacts with Tyr97 α in the TCR CDR3 α loop, as well one hydrogen bond and two van der Waals contacts with Tyr31 β (CDR1 β), and one hydrogen bond and four van der Waals contacts with Trp97 β (CDR3 β ; Fig. 5d). The structural importance of residues Pro5 and Asp6 of the self peptide was consistent with the mutagenesis data (Fig. 2). Thus, the 1E6 TCR is highly focused on a minimal motif dominated by residues Pro5 and Asp6 of the self peptide.

Two CDR3 residues dominate TCR contacts

The central role of residues Pro5 and Asp6 of the self peptide during TCR binding was mirrored by the dominant role of two contact residues in the 1E6 TCR in which Tyr97 α and Trp97 β of the CDR3 α and CDR3 β loops, respectively, dominated the interface (Table 2) and sat directly over the central Gly-Pro-Asp motif of the self peptide (Fig. 5b,d). Every pMHC contact made between the 1E6 TCR α -chain and A2-ALW occurred via a germline-encoded residue (Table 2). Indeed, the 11-residue 1E6 CDR3 α loop was heavily germline encoded, with only three insertions of nontemplated nucleotides encoding Gly93 α . The two CDR3 α -contact residues Asp94 α and Tyr97 α were encoded by *TRAV12-3* and the joining-region gene *TRAJ12*, respectively. The longer-than-average 14-residue CDR3 β loop enabled the formation of a two-turn α -helix, a secondary structure not seen before, to our knowledge, in TCR CDR loops⁴. This unusual α -helix presented the Trp97 β side chain of CDR3 β in the correct orientation to make hydrogen bonds with Asp6 of MHC, stack its aromatic ring against Pro7 and Ala8 of MHC, and make contacts with residues on the MHC α 2-helix. The finding that Trp97 β was the only residue in the CDR3 β loop to contact the self peptide emphasized the importance of this residue in the recognition of A2-ALW (Table 2 and Fig. 5d). The CDR3 β loop was constructed from the products of *TRBV12-4*, *TRBD2* (called 'TRBD2-2' here to reflect the



coding allele) and *TRBJ2-4*, with six insertions of nontemplated nucleotides encoding Trp97 β , Lys99 β and Leu100 β . Tryptophan is rarely found in CDR3 loops, as it is not encoded by the junctional region of any of the 47 genes encoding the TCR α -chain variable region or 54 genes encoding the TCR β -chain variable region. Tryptophan is encoded by just one of 57 TCR α -chain joining-region genes (*TRAJ34*) and is not present in the products of any of the 13 genes encoding the TCR β -chain joining region. Furthermore, tryptophan is also one of just two amino acids encoded by only one of the 64 genetic codons. Thus, the generation of CDR3 loops, including tryptophan, is statistically less probable during variable-diversity-joining recombination. Overall, when the TCR germline-encoded regions and nontemplated nucleotides are considered, tryptophan is the rarest amino acid in CDR3 loops. Furthermore, prominently surface exposed tryptophan residues are often a signature for the mediation of protein-protein interactions³¹. Thus, Trp97 β , in proximity to Tyr97 α , is ideally suited to form a receptor-binding interface; indeed, this combination of residues formed an 'aromatic cap' that dominated TCR contacts with the A2-ALW complex. These highly focused interactions between just two residues of the TCR and two residues of the self peptide governed the antigen specificity of the 1E6 TCR.

DISCUSSION

Despite mounting evidence that MHC class I-restricted CD8⁺ T cells have a pivotal role in the development of type 1 diabetes, the structural and biophysical basis for such an interaction with target beta cells has not been studied. To investigate the molecular basis for the recognition of an HLA-A*0201-restricted PPI epitope (A2-ALW) by a CD8⁺ T cell clone, we solved the structures of the autoreactive 1E6 TCR and A2-ALW in isolation and in complex. Overall, the 1E6 TCR bound to A2-ALW in a canonical diagonal way, with the CDR3 loops positioned over the central bulge of the peptide. Nevertheless, despite this standard docking orientation, the 1E6 TCR engaged A2-ALW with an extremely low affinity, attributable to a lower-than-average buried surface area and limited MHC-contact footprint. Furthermore, several other features of the complex were noteworthy. In contrast to most TCR-pMHC structures determined so far, this autoreactive TCR-self-pMHC interaction was characterized by a rigid 'lock-and-key' conformation more typical of innate receptors

or of natural killer T cell TCR–antigen-presenting molecule CD1d–antigen interactions^{32,33}. Moreover, the interaction was dominated by the CDR3 loops, consistent with a previously proposed system in which non–germline-encoded CDR3 loops drive the energetic landscape of recognition³⁴ yet in conflict with present theories about the role of the CDR1 and CDR2 loops as determinants of MHC restriction^{28,29,35,36}. The findings that patients with type 1 diabetes showed considerable enrichment for T cells specific for this antigen^{20,22} and that 1E6 T cells killed resting beta cells *in vitro* suggest that ultra-low-affinity binding and a highly limited MHC footprint are still sufficient to have an important effect on the destructive processes that lead to insulin deficiency and type 1 diabetes.

Unusually, the 1E6–A2–ALW interaction was focused mainly through just two aromatic TCR residues, with Tyr97 α and Trp97 β accounting for 64% of the contacts. Residue-focused binding was mirrored by the self peptide, in which just two of five TCR contact residues (Pro5 and Asp6) constituted 63% of the contacts. Thus, the interaction between the 1E6 TCR and the ALW peptide was exquisitely focused and was governed by a binding mechanism dominated by just two residues of the TCR and two residues of the self peptide. Aromatic residues, and surface-exposed tryptophan residues in particular, commonly participate in protein–protein interactions³¹ yet are relatively rare in TCR CDR3 loops. Nonetheless, Tyr97 α and Trp97 β seemed to be the driving force in this otherwise weak TCR–pMHC interaction, acting as an aromatic cap that perched on the central region of the self peptide.

There is considerable interest in how T cells bearing TCRs that interact with autoantigens escape negative selection in the thymus and populate the periphery. Comparison of 1E6–A2–ALW and four other self-reactive human TCR–self–pMHC complexes with a typical HLA-A*0201 pathogen-reactive complex emphasized some of the differences in the binding of TCRs to autoimmune and microbial antigens observed so far. These differences suggest several possible mechanisms to explain how self-reactive T cells might escape negative selection. First, a TCR specific for HLA-DR4–MBP has been shown to bind cognate antigen with high affinity and normal topology¹⁴. This is the strongest TCR affinity reported so far for any MHC class II–restricted antigen and is in the range reported for pathogen-specific MHC class I–restricted TCRs²⁴. However, the HLA-DR4–MBP epitope is highly unstable, which has led to the hypothesis that T cells responding to low antigen densities in the thymus could receive a weak signal for positive selection, but then activate in response to higher antigen densities in the periphery. Second, self-reactive TCR–pMHC complexes, such as Ob.1A12–HLA-DR2a–MBP, 3A6–HLA-DR2–MBP and hy.1B11–HLA-DQ–MBP, have unusual conformations relative to those of the more conventional pathogen-specific TCR–pMHC interactions^{13,16,17}. Such unusual TCR–self–pMHC binding orientations may allow T cells bearing these TCRs to bypass negative selection signals. Our own findings suggest a third route of thymic escape. The 1E6 TCR bound A2–ALW conventionally but with a very low affinity that was highly peptide centric. The low affinity of 1E6 TCR may be below the threshold needed to induce negative selection but sufficient to induce killing of beta cells²⁰. We speculate that, for this TCR at least, the presence of cognate self–pMHC in the thymus is very important in terms of selection. It is noteworthy that the *INS* gene encoding PPI is transcribed and translated in the thymus and that having a variable number of tandem repeats of a consensus sequence located 5' of the coding region is the strongest genetic risk for type 1 diabetes outside the MHC³⁷. Homozygosity for alleles containing few repeats (identified by the single-nucleotide polymorphism AA at rs689) confers a relative risk of more than twofold for disease and is associated with 30–50% the

amount of thymic transcription of PPI that occurs in the homozygous protective state (TT at rs689)³⁸. It is proposed that lower thymic *INS* expression impairs central tolerance to PPI, and this paradigm is supported by the demonstration that nonobese diabetic mice with targeted deletion of *Ins2* (the mouse ortholog of *INS*) show enhanced T cell reactivity to insulin and more rapid and penetrant disease³⁹. The patient with type 1 diabetes from whom 1E6 was obtained has AA at rs689. Notably, all three of the mechanisms described above represent atypical recognition parameters that may help self-reactive T cells to bypass thymic deletion.

The observation that clone 1E6 had the lowest affinity of a TCR for pMHC described so far, to our knowledge, yet remained able to kill resting human HLA-A*0201 beta cells with low expression of HLA class I, is a further potentially important finding in the context of disease pathogenesis, as it suggests that such clones have the potential to engage nonconditioned targets. Most disease models of the pathogenesis and initiation of type 1 diabetes proposed so far have suggested that islet inflammation occurs first and that the resulting cytokine-induced islet hyperexpression of HLA class I facilitates CD8⁺ T cell killing. Our data raise the possibility that CD8⁺ T cell killing could be an early event. Preexisting low-affinity CD8⁺ T cells could also be relevant in the setting of islet transplantation, in which donor beta cells have resting expression of HLA class I and therefore constitute targets for 1E6-like CD8⁺ T cells. Similarly, the future use of gene-modified beta cell–replacement therapy may need to include designs that limit the expression of HLA class I to avoid disease recurrence. Finally, our observations raise the consideration of whether 1E6-like autoreactive T cells with ultra-low-affinity TCRs are originally primed by self or non-self ligands. We believe our findings indicate the latter is more likely, especially in the context of many studies suggesting a link among viruses, islet autoimmunity and type 1 diabetes. Extensive searching of databases of viral proteins with the sequence ALWGPDPAAA or modifications tolerated by 1E6 TCR, followed by examination of stimulation of 1E6 *in vitro*, have not shown any potential virus-derived ligands so far (data not shown). However, the number of complete sequences of viruses that might be considered of highest relevance (such as the human enteroviruses) and are in the public domain are limited at present, and pathogen cross-reactivity remains an important question that needs to be addressed. The 1E6 clone recognizes over a million distinct ten–amino acid peptides in the context HLA-A*0201 (ref. 40). A large number of peptides acted as much better agonists than the PPI-derived peptide ALWGPDPAAA. The peptide RQFGPDFPTI was >100-fold more potent than that index self peptide despite differing from the index sequence at seven of ten amino acids. These findings emphasize the potential of TCR degeneracy as a causative factor in autoimmune disease.

In summary, we have presented here the structure of a human TCR in complex with an autoreactive MHC class I–restricted antigen. Collectively, our observations suggest that CD8⁺ T cells expressing the 1E6 TCR could evade negative selection due to a 'light-touch' MHC contact footprint and weak TCR binding. In the periphery, beta cells operating in the presence of higher glucose concentrations, combined with the proinflammatory milieu that leads to hyperexpression of MHC class I, might drive high surface expression of A2–ALW and render such cells susceptible to antigen-experienced, 1E6-like CD8⁺ T cells^{20,41}. Such T cells with low avidity for self probably require priming through contact with an infectious agent. It is possible that the unusual features of the binding of the 1E6 TCR, focusing on just two residues in the self peptide, as seen here, might increase the chances of cross-recognition of pathogen-derived peptides. Indeed, it has been speculated that such 'hot-spot mimicry' limited to a small

number of key features in the TCR-binding footprint could contribute to the initiation of multiple sclerosis⁴². Collectively, these data suggest a mechanism by which 1E6-like CD8⁺ T cells avoid thymic culling to populate the periphery and cause disease.

METHODS

Methods and any associated references are available in the online version of the paper at <http://www.nature.com/natureimmunology/>.

Accession codes. Protein Data Bank: 1E6–A2–ALW complex (P1 space group), 3UTS; 1E6–A2–ALW complex (P₂ space group), 3UTT; 1E6 TCR, 3UTP; A2–ALW, 3UTQ.

Note: Supplementary information is available on the Nature Immunology website.

ACKNOWLEDGMENTS

We thank the staff at Diamond Light Source for facilities and support; M. Zhao for help preparing human islets; and J. Todd for *INS* genotyping. Supported by the Biotechnology and Biological Sciences Research Council (BB/H001085/1), the Wellcome Trust (WT086716 to A.K.S.; WT079848 to L.W.; and WT095767 to D.K.C.), the Juvenile Diabetes Research Foundation (7-2005-877 and 1-2007-1803 to M.P.; and 17-2009-806 to A.K.S., M.P., D.A.P. and A.S.), the European Union Seventh Framework Programme (241447 NAIMIT), the National Institute for Health Research Comprehensive Biomedical Research Center at Guy's & St. Thomas' National Health Service Foundation Trust and King's College London, Research Councils UK (P.J.R.), the National Health and Medical Research Council (J.R.), the Welsh Office of Research and Development (J.J.M.) and the Medical Research Council (D.A.P.).

AUTHOR CONTRIBUTIONS

D.K.C., P.J.R., M.P. and A.K.S., leadership and project conception; D.K.C. and A.M.B., crystallization and surface plasmon resonance studies; D.K.C., A.M.B., F.M., J.J.M., P.J.R. and A.F., data and crystal collection; D.K.C., S.G. and P.J.R., crystallographic analysis; A.S., J.W.D. and R.R.K., cell experiments; G.C.H., preparation of human islets; G.D., T cell culture; E.G., N.L. and P.E.M., cloning of the 1E6 TCR; D.K.C., A.K.S., M.P., P.J.R., J.J.M., J.R. and S.G., manuscript authorship; L.W. and B.K.J., intellectual input; and A.K.S., M.P., D.A.P. and J.R., study funding.

COMPETING FINANCIAL INTERESTS

The authors declare no competing financial interests.

Published online at <http://www.nature.com/natureimmunology/>.

Reprints and permissions information is available online at <http://www.nature.com/reprints/index.html>.

- Nejntsev, S. *et al.* Localization of type 1 diabetes susceptibility to the MHC class I genes HLA-B and HLA-A. *Nature* **450**, 887–892 (2007).
- Wucherpfennig, K.W. & Sethi, D. T cell receptor recognition of self and foreign antigens in the induction of autoimmunity. *Semin. Immunol.* **23**, 84–91 (2011).
- Kappler, J.W., Roehm, N. & Marrack, P. T cell tolerance by clonal elimination in the thymus. *Cell* **49**, 273–280 (1987).
- Rudolph, M.G., Stanfield, R.L. & Wilson, I.A. How TCRs bind MHCs, peptides, and coreceptors. *Annu. Rev. Immunol.* **24**, 419–466 (2006).
- Colf, L.A. *et al.* How a single T cell receptor recognizes both self and foreign MHC. *Cell* **129**, 135–146 (2007).
- Feng, D., Bond, C.J., Ely, L.K., Maynard, J. & Garcia, K.C. Structural evidence for a germline-encoded T cell receptor-major histocompatibility complex interaction 'codon'. *Nat. Immunol.* **8**, 975–983 (2007).
- Sami, M. *et al.* Crystal structures of high affinity human T-cell receptors bound to peptide major histocompatibility complex reveal native diagonal binding geometry. *Protein Eng. Des. Sel.* **20**, 397–403 (2007).
- Borbulevych, O.Y. *et al.* T cell receptor cross-reactivity directed by antigen-dependent tuning of peptide-MHC molecular flexibility. *Immunity* **31**, 885–896 (2009).
- Cole, D.K. *et al.* Germ line-governed recognition of a cancer epitope by an immunodominant human T-cell receptor. *J. Biol. Chem.* **284**, 27281–27289 (2009).
- Gras, S. *et al.* Structural bases for the affinity-driven selection of a public TCR against a dominant human cytomegalovirus epitope. *J. Immunol.* **183**, 430–437 (2009).
- Miles, J.J. *et al.* Genetic and structural basis for selection of a ubiquitous T cell receptor deployed in Epstein-Barr virus infection. *PLoS Pathog.* **6**, e1001198 (2010).
- Borbulevych, O.Y., Piepenbrink, K.H. & Baker, B.M. Conformational melding permits a conserved binding geometry in TCR recognition of foreign and self molecular mimics. *J. Immunol.* **186**, 2950–2958 (2011).
- Sethi, D.K. *et al.* A highly tilted binding mode by a self-reactive T cell receptor results in altered engagement of peptide and MHC. *J. Exp. Med.* **208**, 91–102 (2011).
- Yin, Y., Li, Y., Kerzic, M.C., Martin, R. & Mariuzza, R.A. Structure of a TCR with high affinity for self-antigen reveals basis for escape from negative selection. *EMBO J.* **30**, 1137–1148 (2011).
- Godfrey, D.I., Rossjohn, J. & McCluskey, J. The fidelity, occasional promiscuity, and versatility of T cell receptor recognition. *Immunity* **28**, 304–314 (2008).
- Hahn, M., Nicholson, M.J., Pyrdol, J. & Wucherpfennig, K.W. Unconventional topology of self peptide-major histocompatibility complex binding by a human autoimmune T cell receptor. *Nat. Immunol.* **6**, 490–496 (2005).
- Li, Y. *et al.* Structure of a human autoimmune TCR bound to a myelin basic protein self-peptide and a multiple sclerosis-associated MHC class II molecule. *EMBO J.* **24**, 2968–2979 (2005).
- Willcox, A., Richardson, S.J., Bone, A.J., Foulis, A.K. & Morgan, N.G. Analysis of islet inflammation in human type 1 diabetes. *Clin. Exp. Immunol.* **155**, 173–181 (2009).
- DiLorenzo, T.P. & Serreze, D.V. The good turned ugly: immunopathogenic basis for diabetogenic CD8⁺ T cells in NOD mice. *Immunity Rev.* **204**, 250–263 (2005).
- Skowera, A. *et al.* CTLs are targeted to kill beta cells in patients with type 1 diabetes through recognition of a glucose-regulated preproinsulin epitope. *J. Clin. Invest.* **118**, 3390–3402 (2008).
- Foulis, A.K., Farquharson, M.A. & Meager, A. Immunoreactive α -interferon in insulin-secreting beta cells in type 1 diabetes mellitus. *Lancet* **2**, 1423–1427 (1987).
- Velthuis, J.H. *et al.* Simultaneous detection of circulating autoreactive CD8⁺ T-cells specific for different islet cell-associated epitopes using combinatorial MHC multimers. *Diabetes* **59**, 1721–1730 (2010).
- Cole, D.K. *et al.* Modification of MHC anchor residues generates heteroclitic peptides that alter TCR binding and T cell recognition. *J. Immunol.* **185**, 2600–2610 (2010).
- Cole, D.K. *et al.* Human TCR-binding affinity is governed by MHC class restriction. *J. Immunol.* **178**, 5727–5734 (2007).
- Armstrong, K.M., Piepenbrink, K.H. & Baker, B.M. Conformational changes and flexibility in T-cell receptor recognition of peptide-MHC complexes. *Biochem. J.* **415**, 183–196 (2008).
- Tynan, F.E. *et al.* A T cell receptor flattens a bulged antigenic peptide presented by a major histocompatibility complex class I molecule. *Nat. Immunol.* **8**, 268–276 (2007).
- Tynan, F.E. *et al.* T cell receptor recognition of a 'super-bulged' major histocompatibility complex class I-bound peptide. *Nat. Immunol.* **6**, 1114–1122 (2005).
- Dai, S. *et al.* Crossreactive T Cells spotlight the germline rules for $\alpha\beta$ T cell-receptor interactions with MHC molecules. *Immunity* **28**, 324–334 (2008).
- Wu, L.C., Tuot, D.S., Lyons, D.S., Garcia, K.C. & Davis, M.M. Two-step binding mechanism for T-cell receptor recognition of peptide MHC. *Nature* **418**, 552–556 (2002).
- Burrows, S.R. *et al.* Hard wiring of T cell receptor specificity for the major histocompatibility complex is underpinned by TCR adaptability. *Proc. Natl. Acad. Sci. USA* **107**, 10608–10613 (2010).
- Pang, S.S. *et al.* The structural basis for autonomous dimerization of the pre-T-cell antigen receptor. *Nature* **467**, 844–848 (2010).
- Borg, N.A. *et al.* CD1d-lipid-antigen recognition by the semi-invariant NKT T-cell receptor. *Nature* **448**, 44–49 (2007).
- Godfrey, D.I. *et al.* Antigen recognition by CD1d-restricted NKT T cell receptors. *Semin. Immunol.* **22**, 61–67 (2010).
- Borg, N.A. *et al.* The CDR3 regions of an immunodominant T cell receptor dictate the 'energetic landscape' of peptide-MHC recognition. *Nat. Immunol.* **6**, 171–180 (2005).
- Garcia, K.C., Adams, J.J., Feng, D. & Ely, L.K. The molecular basis of TCR germline bias for MHC is surprisingly simple. *Nat. Immunol.* **10**, 143–147 (2009).
- Scott-Browne, J.P., White, J., Kappler, J.W., Gapin, L. & Marrack, P. Germline-encoded amino acids in the $\alpha\beta$ T-cell receptor control thymic selection. *Nature* **458**, 1043–1046 (2009).
- Todd, J.A. *et al.* Robust associations of four new chromosome regions from genome-wide analyses of type 1 diabetes. *Nat. Genet.* **39**, 857–864 (2007).
- Pugliese, A. *et al.* The insulin gene is transcribed in the human thymus and transcription levels correlated with allelic variation at the INS VNTR-IDDM2 susceptibility locus for type 1 diabetes. *Nat. Genet.* **15**, 293–297 (1997).
- Thébault-Baumont, K. *et al.* Acceleration of type 1 diabetes mellitus in proinsulin 2-deficient NOD mice. *J. Clin. Invest.* **111**, 851–857 (2003).
- Wooldridge, L. *et al.* A single autoimmune T-cell receptor recognizes over a million different peptides. *J. Biol. Chem.* **287**, 1168–1177 (2012).
- Foulis, A.K., Farquharson, M.A. & Hardman, R. Aberrant expression of class II major histocompatibility complex molecules by B cells and hyperexpression of class I major histocompatibility complex molecules by insulin containing islets in type 1 (insulin-dependent) diabetes mellitus. *Diabetologia* **30**, 333–343 (1987).
- Harkioliaki, M. *et al.* T cell-mediated autoimmune disease due to low-affinity crossreactivity to common microbial peptides. *Immunity* **30**, 348–357 (2009).

ONLINE METHODS

Cytotoxicity assays. Human islet cells were isolated as described⁴³. Pancreata were retrieved with the consent of donors' relatives and permission from the Ethical Review Committee of King's College Hospital. Islet-enriched cell fractions were cultured for 2 weeks in CMRL-1066 medium containing 5.6 mM glucose, supplemented with 10% (vol/vol) FBS, penicillin (100 U/ml), streptomycin (100 µg/ml) and L-glutamine (2 mM; Invitrogen). Cells were allowed to become monolayer cultures and were cultured for 16–24 h with 16 mM glucose in the presence or absence of interleukin 1β (50 IU/ml; Strathmann Biotec), tumor necrosis factor (2,500 IU/ml), interferon-γ (500 IU/ml; Miltenyi Biotec) and interferon-α (1,000 IU/ml; Roche Laboratories) for upregulation of the expression of HLA class I. Cytotoxicity was analyzed with a nonradioactive europium thiodiglycolate cytotoxicity assay by DELFIA Technology according to the manufacturer's instructions (PerkinElmer). Human islet cells (1×10^6) were incubated for 20 min at 37 °C in 2 ml CMRL-1066 medium with 3 µl fluorescence-enhancing ligand. After cells were washed three times with PBS, 50 µl labeled islet cells (5×10^3) were seeded in triplicate into V-shaped 96-well plates, followed by the addition of 50 µl effector cells (CD8⁺ T cell clone) at various ratios of effector cells to target cells in X-VIVO 15 medium and 5% (vol/vol) AB serum containing interleukin 7 (10 ng/ml), interleukin 15 (0.1 ng/ml) and 2.5% (vol/vol) Cellkines (Helvetica Healthcare). Cultures were incubated for 4 h at 37 °C, then 20 µl supernatant was transferred to a clear, flat-bottom microtitration plate followed by the addition of enhancement solution (200 µl/well). After 15 min at 20–22 °C with shaking, the europium signal was measured with a FLUOstar OMEGA Time-Resolved Fluorescence reader (BMG Labtech). For analysis of maximum lysis, islet cells alone (5×10^3 in a volume of 100 µl) were treated with 20 µl lysis buffer. Spontaneous release was measured in wells containing only labeled islet cells in 100 µl of medium. Specific cytotoxicity was calculated with the following formula: percent specific release = (experimental release – spontaneous release) × 100 / (maximum release – spontaneous release).

Peptide-mutagenesis scan of 1E6 T cells. For the recognition screen, 2×10^3 1E6 CD8⁺ T cells were cultured for 16 h in triplicate with individual peptides representing every positional variant ($n = 190$) of the wild-type PPI epitope sequence (ALWGPDPAAA; amino acids 15–24), at a concentration of 1 µg/ml. Supernatants were collected and analyzed for the production of tumor necrosis factor by enzyme-linked immunosorbent assay according to the manufacturer's instructions (Life Technologies).

Generation of CD8⁺ T cell clones and expression plasmids. CD8⁺ T cell clones specific for A2-ALW were generated as described²⁰. Sequences encoding the 1E6 TCR, HLA-A*0201 α-chain and β₂-microglobulin were generated by PCR mutagenesis (Stratagene) and PCR cloning. For the 1E6 TCR, a disulfide-linked construct was used for production of the soluble domains (variable and constant) for both the α-chain and β-chain⁴⁴. The soluble HLA-A*0201 α-chain (α1, α2 and α3 domains), tagged with a biotinylation sequence, and β₂-microglobulin were also cloned and used to make HLA-A*0201. Sequences encoding the TCR α-chain and β-chain, HLA-A*0201 α-chain and β₂-microglobulin were inserted into separate pGMT7 expression plasmids under the control of the T7 promoter.

Protein expression, refolding and purification. Competent Rosetta DE3 *Escherichia coli* cells were used for production of the 1E6 TCR α-chain and β-chain, and the HLA-A*0201 α-chain and β₂-microglobulin, in the form of inclusion bodies, with 0.5 mM isopropyl β-D-thiogalactopyranoside to induce expression as described⁴⁴. TCR and pMHCI proteins were refolded as described²⁴. Refolded proteins were purified initially by ion exchange with a Poros50HQ column and were finally resolved by gel filtration into BIAcore buffer (10 mM HEPES, pH 7.4, 150 mM NaCl, 3 mM EDTA and 0.005% (vol/vol) Surfactant P20) or crystallization buffer (10 mM Tris, pH 8.1, and

10 mM NaCl) with a Superdex200HR column. Protein quality was analyzed by SDS-PAGE followed by Coomassie staining.

Biotinylation of pMHC. Biotinylated pMHC was prepared as described⁴⁵.

Surface plasmon resonance analysis. Binding was analyzed with a BIAcore T100 equipped with a CM5 sensor chip as reported⁴⁵. Between 200 and 400 response units of biotinylated pMHC were immobilized onto streptavidin, which was chemically linked to the chip surface. Equilibrium analysis was done with ten serial dilutions prepared in triplicate for each sample and injected over the relevant sensor chips at 25 °C. The 1E6 TCR was injected over the chip surface with kinetic injections at a flow rate of 45 µl/min. For analysis of temperature dependence, this method was repeated at 5 °C and 37 °C. Results were analyzed with BIAevaluation 3.1 software, Microsoft Excel and Origin 6.1 software. The equilibrium binding constant values were calculated with the following nonlinear curve fit: $y = (P_1x) / (P_2 + x)$, where 'y' represents response units, 'P₁' represents the maximal response units when the surface bound pMHC is saturated by the injected TCR, 'P₂' represents the dissociation constant and 'x' represents molar concentration of the TCR.

Crystallization, diffraction data collection and model refinement. Crystals of 1E6-A2-ALW, the 1E6 TCR and A2-ALW were grown at 18 °C by vapor diffusion by the sitting-drop technique. For 1E6-A2-ALW, optimal crystals were obtained with 0.2 M sodium citrate, 0.1 M Bis-Tris propane, pH 6.5, and 20% (wt/vol) polyethylene glycol 3350. For A2-ALW, optimal crystals were obtained with 0.2 M potassium-sodium tartrate, 0.1 M Bis-Tris propane, pH 6.5, and 20% (wt/vol) polyethylene glycol 3350. For the 1E6 TCR, optimal crystals were obtained with 0.2 M sodium iodide and 20% (wt/vol) polyethylene glycol 3350. All crystals were soaked in 30% (vol/vol) ethylene glycol before being flash-frozen in liquid nitrogen at –190 °C ('cryo-cooling'). All crystallization screens and optimization experiments were completed with an Art-Robbins Phoenix dispensing robot (Alpha Biotec). Data were collected at 100K at the Diamond Light Source. All data sets were collected at a wavelength of 0.976 Å with an ADSC Q315 charge-coupled device detector. Reflection intensities were estimated with the xia2 data-reduction system for crystallography⁴⁶, and the data were scaled, reduced and analyzed with the Scala program (scale together multiple observations of reflections) of the CCP4 package (Collaborative Computational Project number 4)⁴⁷. The structure was solved with the molecular-replacement program AMoRe⁴⁸. The model sequence was adjusted with the COOT program for macromolecular model building, completion and confirmation (Crystallographic Object-Oriented Toolkit)⁴⁹ and the model was refined with the REFMAC5 macromolecular refinement program. Graph presentations were prepared with the PyMOL molecular graphics system⁵⁰. Data reduction and refinement statistics are presented in **Supplementary Table 1**.

43. Huang, G.C. et al. The development of new density gradient media for purifying human islets and islet-quality assessments. *Transplantation* **77**, 143–145 (2004).
44. Boulter, J.M. et al. Stable, soluble T-cell receptor molecules for crystallization and therapeutics. *Protein Eng.* **16**, 707–711 (2003).
45. Cole, D.K. et al. T cell receptor engagement of peptide-major histocompatibility complex class I does not modify CD8 binding. *Mol. Immunol.* **45**, 2700–2709 (2008).
46. Winter, G. xia2: an expert system for macromolecular crystallography data reduction. *J. Appl. Crystallogr.* **43**, 186–190 (2010).
47. Collaborative Computational Project. N. The CCP4 suite: programs for protein crystallography. *Acta Crystallogr. D Biol. Crystallogr.* **50**, 760–763 (1994).
48. Trapani, S. & Navaza, J. AMoRe: classical and modern. *Acta Crystallogr. D Biol. Crystallogr.* **64**, 11–16 (2008).
49. Emsley, P. & Cowtan, K. Coot: model-building tools for molecular graphics. *Acta Crystallogr. D Biol. Crystallogr.* **60**, 2126–2132 (2004).
50. Delano, W.L. *The PyMOL Molecular Graphics System* (DeLano Scientific, San Carlos, California, 2002).